THE SHAPE OF SPECTRAL BREAKS IN GAMMA-RAY BURST AFTERGLOWS

Jonathan Granot[1,2] and Re'em Sari[3]

ABSTRACT

Gamma-ray burst afterglows are well described by synchrotron emission from relativistic blast waves expanding into an external medium. The blast wave is believed to amplify the magnetic field and accelerate the electrons into a power-law distribution of energies promptly behind the shock. These electrons then cool both adiabatically and by emitting synchrotron and inverse Compton radiation. The resulting spectra are known to consist of several power-law segments, which smoothly join at certain break frequencies. Here, we give a complete description of all possible spectra under those assumptions and find that there are five possible regimes, depending on the ordering of the break frequencies. The flux density is calculated by integrating over all of the contributions to a given photon arrival time from all of the shocked region using the Blandford & McKee solution. This allows us to calculate more accurate expressions for the value of these break frequencies and describe the shape of the spectral breaks around them. This also provides the shape of breaks in the light curves caused by the passage of a break frequency through the observed band. These new, more exact, estimates are different from more simple calculations by typically a factor of a few, and they describe some new regimes that were previously ignored.

Subject headings: gamma rays: bursts — gamma rays: theory — radiation mechanisms: nonthermal — shock waves

1. INTRODUCTION

In recent years, several dozen gamma-ray burst (GRB) afterglows have been observed, and data are accumulating rapidly. The quality of these observations is constantly improving. The study of afterglow emission has helped shed light on many important aspects of the GRB phenomenon. The spectrum during the afterglow phase is well described by synchrotron emission from a relativistic blast wave and consists of several power-law segments (PLSs) that join at several break frequencies (e.g., Sari, Piran, & Narayan 1998). These break frequencies are the self-absorption frequency, ν_{sa}, below which the optical depth to synchrotron self-absorption is larger than unity, ν_m, the typical synchrotron frequency of the minimal electron in the power law, and ν_c, the synchrotron frequency of an electron whose cooling time equals the dynamical time of the system. Granot, Piran, & Sari (2000) then found that if $\nu_c < \nu_m$, the self-absorption frequency actually splits in two: ν_{ac} and ν_{sa}, where an optical depth of unity is produced by noncooled electrons and all electrons, respectively. Different possible orderings of these break frequencies result in five possible spectral regimes, as shown in Figure 1.

The physical parameters of a burst may be deduced from fitting the observed broadband spectrum to the theoretical spectrum. This has been done by Wijers & Galama (1999) for GRB 970508 by fitting a broken power-law theoretical spectrum. A detailed description of the shape of the spectrum allowed a more accurate determination of the self-absorption frequency ν_{sa} and the peak frequency ν_m (Granot, Piran, & Sari 1999b, hereafter GPS99b). A more accurate theoretical calculation of the break frequencies

leads to a more accurate conversion from the observed spectrum to the burst parameters. The combined effect was that the inferred value of the density, for example, was different than that of Wijers & Galama (1999) by 2 orders of magnitude. This illustrates the sensitivity of this method to the shape of the theoretical spectrum around the break points and stresses the need for a more accurate determination of the theoretical break frequencies for all various spectral breaks.

So far, only the shape of the spectrum around ν_m (Granot, Piran, & Sari 1999a, hereafter GPS99a; Gruzinov & Waxman 1999) and ν_{sa} (GPS99b) was calculated in detail, and even that was done only for the canonical case, where $\nu_{sa} < \nu_m < \nu_c$ (*upper panel*, Fig. 1). This paper is intended to extend these works for *all* spectral breaks and therefore to provide a comprehensive, self-consistent calculation of the broadband spectrum. We provide analytic formulae that approximate the shape of each of the spectral breaks and their positions in a form that is easy to use for afterglow fitting. We also suggest a prescription for combining these breaks to a single analytic broadband spectrum.

The physical model is outlined in § 2, while a more detailed and formal description of the model and of the calculation of the observed flux density is given in the Appendix. Our main results are presented in § 3. In § 4, we give prescriptions for combining the shapes of the spectrum near the different spectral breaks into a single analytic broadband spectrum. We discuss our results in § 5.

2. PHYSICAL MODEL

An exact calculation of the spectrum requires the knowledge of (1) the hydrodynamic quantities (bulk Lorentz factor and number density), (2) the magnetic field strength, and (3) the electron energy distribution. These should be given for any location behind the shock and at any time. Below, we describe our approach to all three.

[1] Racah Institute of Physics, Hebrew University, Jerusalem 91904, Israel.
[2] Institute for Advanced Study, Olden Lane, Princeton, NJ 08540.
[3] Theoretical Astrophysics 130-33, California Institute of Technology, Pasadena, CA 91125.
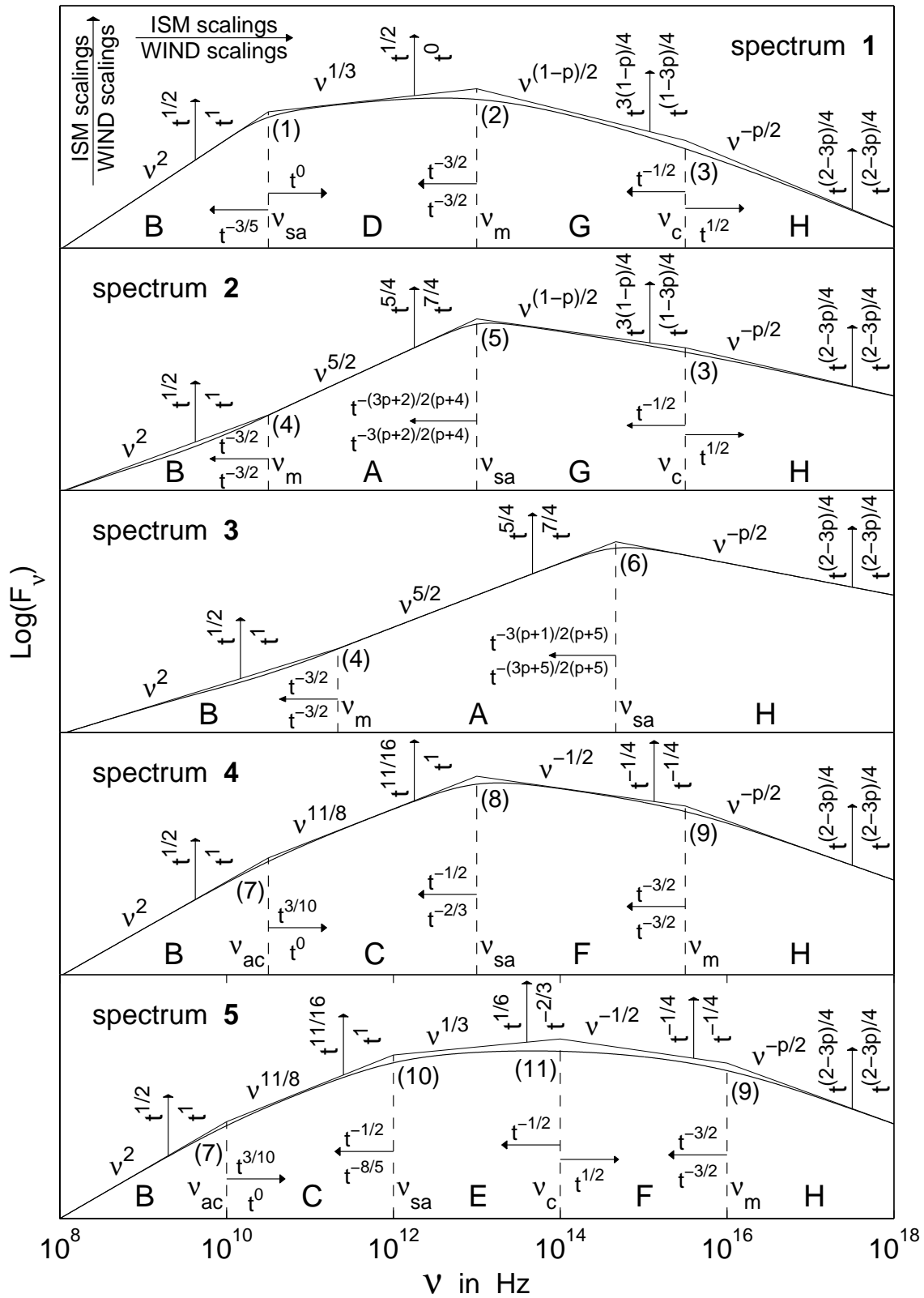
Fig. 1.—Different possible broadband synchrotron spectra from a relativistic blast wave that accelerates the electrons to a power-law distribution of energies. The thin solid line shows the asymptotic PLSs and their points of intersection, where the break frequencies, ν_b, and the corresponding flux densities, $F_{\nu_b,\text{ext}}$, are defined. The different PLSs are labeled A–H, while the different break frequencies are labeled 1–11. The temporal scalings of the PLSs and the break frequencies for an ISM ($k = 0$) or stellar wind ($k = 2$) environment are indicated by the arrows. The thick solid line shows the spectrum we calculated in this paper, where the broadband spectrum is constructed according to the prescription suggested in § 4. The different spectra are labeled 1–5 from top to bottom. The relevant spectrum is determined by the ordering of the break frequencies. The top two panels (spectra 1 and 2) correspond to slow cooling ($\nu_m < \nu_c$). Spectrum 1 applies when $\nu_{sa} < \nu_m$, while spectrum 2 applies when $\nu_m < \nu_{sa} < \nu_c$. The two bottom panels (spectra 4 and 5) correspond to fast cooling ($\nu_c < \nu_m$). Spectrum 5 applies when $\nu_{sa} < \nu_c$, and spectrum 4 applies when $\nu_c < \nu_{sa} < \nu_m$. Spectrum 3 (*middle panel*) applies when $\nu_{sa} > \nu_m$, ν_c, where in this case the relative ordering of ν_c and ν_m is unimportant (i.e., spectrum 3 may apply to slow cooling or fast cooling).

1. The hydrodynamics is described by the Blandford & McKee (1976, hereafter BM) self-similar solution. This solution describes a spherical relativistic blast wave expanding into a cold medium and assumes an adiabatic flow, i.e., that radiation losses are small and do not effect the hydrodynamics. Radiative effects can be taken into account to modify the hydrodynamic evolution, as described by Sari (1997) and Cohen, Piran, & Sari (1998), and to modify the structure of the cooling layer behind the shock, as described by Granot & Königl (2001). If the radiative losses are not too large, our formalism would give the correct break frequencies and break shapes, provided that one uses the time-dependent energy, as discussed in the first two of these references. The BM solution we use is for an impulsive explosion in an ambient density described by a power law with radius $\rho_{\rm ext}(r) = Ar^{-k}$. We consider two different values of k that are of particular physical interest: $k = 0$, corresponding to an interstellar medium (ISM), and $k = 2$, corresponding to a massive star progenitor surrounded by its preexplosion wind. The assumption of a spherical flow is also adequate for a jetted flow at sufficiently early times, when the Lorentz factor of the flow is still larger than the inverse opening angle of the jet. We therefore have the complete hydrodynamic description in terms of the total energy E and the external number density $n_{\rm ext}$ (or A in the case of wind). The hydrodynamic profile used is given in equations (A4), (A5), and (A6).

2. We assume that the magnetic field gets a fixed fraction, ϵ_B, of the internal energy everywhere behind the shock, as given by equation (A2). This would be the case if the shock-amplified, randomly oriented magnetic field decreases as a result of adiabatic expansion. Different assumptions on the evolution and orientation of the magnetic field were shown to have only a small effect on the resulting spectrum (GPS99a; GPS99b).

3. The electrons are assumed to acquire a power-law distribution of energies, $N(\gamma) \propto \gamma^{-p}$ for $\gamma \geq \gamma_{\rm min,0}$, immediately behind the shock. Their total energy immediately behind the shock is a fraction ϵ_e of the internal energy. After being accelerated by the shock, the electrons cool because of radiative losses and adiabatic cooling. The former can be calculated from synchrotron theory and the latter from the density profile given by the BM solution. The resulting distribution is given in equation (A13).

Given the above, the observed flux density may be calculated as described in the Appendix. The spectrum for the optically thin breaks may be calculated using equation (A14), while equation (A24) applies more generally. In both cases, the contributions from all of the shocked regions from photons that reach the observer simultaneously are taken into account when calculating the flux density.

3. RESULTS

Power-law segments.—All five possible different spectra, which are shown in Figure 1, consist of between three and five different PLSs. At each asymptotic PLS (sufficiently far from the break frequencies) we have $F_\nu \propto \nu^\beta t^\alpha$. Altogether there are eight different PLSs, labeled A through H, from high to low values of β. Note that there are two different PLSs with a slope of $\beta = \frac{1}{3}$. Both are produced by the low-energy tail of synchrotron radiation, but in region D it is the noncooled electrons that are responsible for the radiation,

while in region E it is the cooled electrons. Most PLSs appear in more than one of the five possible spectra (see Fig. 1). If one is interested only in the spectrum far enough from the break frequencies, then the normalizations of the different PLSs are all that is needed to accurately describe the spectrum. This is given in Table 1. The coefficients for PLSs A, G, and H depend slightly on p in a nonanalytic way. These were calculated for $p = 2.2$, 2.5, and 3, and a linear function (or a linear function multiplied by an exponent) was used to describe the results.

For PLS E, we find that the emission becomes dominated by the contribution from small radii (i.e., early times when the radius of the shock was small) for $k \geq 23/13 \approx 1.769$. The electrons responsible for the emission in this regime have suffered considerable adiabatic cooling (as well as radiative losses). In this regime ($k > 23/13$), PLS E splits into two different PLSs, whose spectral slope β depends on k. Furthermore, the effective size of the afterglow image at a given observed time in this regime depends on the observed frequency. Since this new regime is somewhat out of the main stream of this paper, however, and in order to avoid confusion, we leave the detailed description of this new regime to a future work (J. Granot & R. Sari 2002, in preparation). The normalization of PLS E and the expressions for the spectral breaks $b = 10$, 11 (that involve PLS E) are therefore left out of Tables 1 and 2, respectively, for $k = 2$.

Break frequencies.—The different possible combinations of the eight PLSs result in 11 different break frequencies labeled $b = 1, \ldots, 11$ (see Fig. 1). Again, the same break frequency can appear in more than one spectrum. The values of the break frequencies, ν_b, and the corresponding extrapolated flux densities, $F_{\nu_b, \rm ext}$, are defined at the point where the asymptotic PLSs meet. These can be calculated directly from the normalization of the PLSs that are given in Table 1, but for completeness they are given explicitly in Table 2. The fit for the p dependence was redone in this table (with either a linear fit, an exponent, or a combination of the two) using the accurate results for $p = 2.2$, 2.5, 3, therefore resulting in slight (a few percent) inconsistencies with the previous table.

Shape of breaks.—The flux density near a spectral break, ν_b, may be approximated by

$$F_\nu = F_{\nu_b, \rm ext} \left[\left(\frac{\nu}{\nu_b} \right)^{-s\beta_1} + \left(\frac{\nu}{\nu_b} \right)^{-s\beta_2} \right]^{-1/s}, \qquad (1)$$

where β_1 and β_2 are the asymptotic spectral slopes below and above the break, respectively, and s is a parameter that describes the sharpness of each break. The sign of s is equal to that of $\beta_1 - \beta_2$ (i.e., positive if the spectral slope decreases across the break), while $|s|$ represents the sharpness of the break (the sharper the break, the larger $|s|$). The shape of most spectral breaks (except for $b = 1$, 8, 10, 11) depends on the value of p, as does the corresponding value of $s = s(p)$, which is given in Table 2. All quantities that depend on the value of p were calculated for $p = 2.2$, 2.5, 3 and are given in a form that is as exact as the functional parameterization permits at these values of p and interpolates (or extrapolates) for other values of p; these values should therefore be reasonably accurate for $1.5 \lesssim p \lesssim 3.5$ (see discussion below eq. [A1] for $p < 2$).

The break $b = 1$ has been investigated in detail by GPS99a for $k = 0$, and they found that the physically

TABLE 1
Normalization of the Different Power-Law Segments

PLS	β	$F_\nu(k=0)$ (mJy)	$F_\nu(k=2)$ (mJy)
A.......	$5/2$	$1.18(4.59-p)10^8(1+z)^{9/4}\epsilon_B^{-1/4}n_0^{-1/2}E_{52}^{1/4}t_{\rm days}^{5/4}d_{L28}^{-2}\nu_{14}^{5/2}$	$2.96(4.59-p)10^7(1+z)^{7/4}\epsilon_B^{-1/4}A_*^{-1}E_{52}^{3/4}t_{\rm days}^{7/4}d_{L28}^{-2}\nu_{14}^{5/2}$
B.......	2	$4.20\dfrac{3p+2}{3p-1}10^9(1+z)^{5/2}\bar{\epsilon}_e n_0^{-1/2}E_{52}^{1/2}t_{\rm days}^{1/2}d_{L28}^{-2}\nu_{14}^2$	$1.33\dfrac{3p+2}{3p-1}10^9(1+z)^2\bar{\epsilon}_e A_*^{-1}E_{52}t_{\rm days}d_{L28}^{-2}\nu_{14}^2$
C.......	$11/8$	$8.01\times10^5(1+z)^{27/16}\epsilon_B^{-1/4}n_0^{-5/16}E_{52}^{7/16}t_{\rm days}^{11/16}d_{L28}^{-2}\nu_{14}^{11/8}$	$3.28\times10^5(1+z)^{11/8}\epsilon_B^{-1/4}A_*^{-5/8}E_{52}^{3/4}t_{\rm days}d_{L28}^{-2}\nu_{14}^{11/8}$
D......	$1/3$	$27.9\dfrac{p-1}{3p-1}(1+z)^{5/6}\bar{\epsilon}_e^{-2/3}\epsilon_B^{1/3}n_0^{1/2}E_{52}^{5/6}t_{\rm days}^{1/2}d_{L28}^{-2}\nu_{14}^{1/3}$	$211\dfrac{p-1}{3p-1}(1+z)^{4/3}\bar{\epsilon}_e^{-2/3}\epsilon_B^{1/3}A_*E_{52}^{1/3}d_{L28}^{-2}\nu_{14}^{1/3}$
E.......	$1/3$	$73.0(1+z)^{7/6}\epsilon_B n_0^{5/6}E_{52}^{7/6}t_{\rm days}^{1/6}d_{L28}^{-2}\nu_{14}^{1/3}$	$\cdots$ [a]
F.......	$-1/2$	$6.87(1+z)^{3/4}\epsilon_B^{-1/4}E_{52}^{3/4}t_{\rm days}^{-1/4}d_{L28}^{-2}\nu_{14}^{-1/2}$	$6.68(1+z)^{3/4}\epsilon_B^{-1/4}E_{52}^{3/4}t_{\rm days}^{-1/4}d_{L28}^{-2}\nu_{14}^{-1/2}$
G......	$(1-p)/2$	$0.461(p-0.04)e^{2.53p}(1+z)^{(3+p)/4}\bar{\epsilon}_e^{p-1}\epsilon_B^{(1+p)/4}n_0^{1/2}E_{52}^{(3+p)/4}t_{\rm days}^{3(1-p)/4}d_{L28}^{-2}\nu_{14}^{(1-p)/2}$	$3.82(p-0.18)e^{2.54p}(1+z)^{(5+p)/4}\bar{\epsilon}_e^{p-1}\epsilon_B^{(1+p)/4}A_*E_{52}^{(1+p)/4}t_{\rm days}^{(1-3p)/4}d_{L28}^{-2}\nu_{14}^{(1-p)/2}$
H......	$-p/2$	$0.855(p-0.98)e^{1.95p}(1+z)^{(2+p)/4}\bar{\epsilon}_e^{p-1}\epsilon_B^{(p-2)/4}E_{52}^{(2+p)/4}t_{\rm days}^{(2-3p)/4}d_{L28}^{-2}\nu_{14}^{-p/2}$	$0.0381(7.11-p)e^{2.76p}(1+z)^{(2+p)/4}\bar{\epsilon}_e^{p-1}\epsilon_B^{(p-2)/4}E_{52}^{(2+p)/4}t_{\rm days}^{(2-3p)/4}d_{L28}^{-2}\nu_{14}^{-p/2}$

NOTE.—First two columns give the labels and the spectral slope, β, of the different PLSs (see Fig. 1), while the last two columns give the asymptotic flux density within each PLS for $k=0$ and $k=2$. The reader is reminded that $\bar{\epsilon}_e = \epsilon_e(p-2)/(p-1)$ depends on p. The notation Q_x stands for the quantity Q in units of 10^x times the (cgs) units of Q, while $t_{\rm days}$ is the observed time in days, and A_* is A in units of 5×10^{11} g cm^{-1} (Chevalier & Li 2000).

[a] For PLS E, the emission becomes dominated by the contribution from small radii for $k>23/13$. This new regime is described in a separate work (J. Granot & R. Sari 2002, in preparation).

TABLE 2
Break Frequencies and Corresponding Flux Densities

b	β_1	β_2	ν_b	$\nu_b(p)$ (Hz)	$F_{\nu_b,{\rm ext}}(p)$ (mJy)	$s(p)$	MRD (%)
1.....	2	$\dfrac{1}{3}$	$\nu_{\rm sa}$	$1.24\dfrac{(p-1)^{3/5}}{(3p+2)^{3/5}}10^9(1+z)^{-1}\bar{\epsilon}_e^{-1}\epsilon_B^{1/5}n_0^{3/5}E_{52}^{1/5}$	$0.647\dfrac{(p-1)^{6/5}}{(3p-1)(3p+2)^{1/5}}(1+z)^{1/2}\bar{\epsilon}_e^{-1}\epsilon_B^{2/5}n_0^{7/10}E_{52}^{9/10}t_{\rm days}^{1/2}d_{L28}^{-2}$	1.64	6.68
				$8.31\dfrac{(p-1)^{3/5}}{(3p+2)^{3/5}}10^9(1+z)^{-2/5}\bar{\epsilon}_e^{-1}\epsilon_B^{1/5}A_*^{6/5}E_{52}^{-2/5}t_{\rm days}^{-3/5}$	$9.19\dfrac{(p-1)^{6/5}}{(3p-1)(3p+2)^{1/5}}(1+z)^{6/5}\bar{\epsilon}_e^{-1}\epsilon_B^{2/5}A_*^{7/5}E_{52}^{1/5}t_{\rm days}^{-1/5}d_{L28}^{-2}$	1.06	1.02
2.....	$\dfrac{1}{3}$	$\dfrac{1-p}{2}$	ν_m	$3.73(p-0.67)10^{15}(1+z)^{1/2}E_{52}^{1/2}\bar{\epsilon}_e^2\epsilon_B^{1/2}t_{\rm days}^{-3/2}$	$9.93(p+0.14)(1+z)\epsilon_B^{1/2}n_0^{1/2}E_{52}d_{L28}^{-2}$	$1.84-0.40p$	5.9
				$4.02(p-0.69)10^{15}(1+z)^{1/2}E_{52}^{1/2}\bar{\epsilon}_e^2\epsilon_B^{1/2}t_{\rm days}^{-3/2}$	$76.9(p+0.12)(1+z)^{3/2}\epsilon_B^{1/2}A_*E_{52}^{1/2}t_{\rm days}^{-1/2}d_{L28}^{-2}$	$1.76-0.38p$	7.2
3.....	$\dfrac{1-p}{2}$	$-\dfrac{p}{2}$	ν_c	$6.37(p-0.46)10^{13}e^{-1.16p}(1+z)^{-1/2}\epsilon_B^{-3/2}n_0^{-1}E_{52}^{-1/2}t_{\rm days}^{-1/2}$	$4.68e^{4.82(p-2.5)}10^3(1+z)^{(p+1)/2}\bar{\epsilon}_e^{p-1}\epsilon_B^{p-1/2}n_0^{p/2}E_{52}^{(p+1)/2}t_{\rm days}^{(1-p)/2}d_{L28}^{-2}$	$1.15-0.06p$	1.9
				$4.40(3.45-p)10^{10}e^{0.45p}(1+z)^{-3/2}\epsilon_B^{-3/2}A_*^{-2}E_{52}^{1/2}t_{\rm days}^{1/2}$	$8.02e^{7.02(p-2.5)}10^5(1+z)^{p+1/2}\bar{\epsilon}_e^{p-1}\epsilon_B^{p-1/2}A_*^p E_{52}^{1/2}t_{\rm days}^{1/2-p}d_{L28}^{-2}$	$0.80-0.03p$	4.4
4.....	2	$\dfrac{5}{2}$	ν_m	$5.04(p-1.22)10^{16}(1+z)^{1/2}\bar{\epsilon}_e^2\epsilon_B^{1/2}E_{52}^{1/2}t_{\rm days}^{-3/2}$	$3.72(p-1.79)10^{15}(1+z)^{7/2}\bar{\epsilon}_e^5\epsilon_B n_0^{-1/2}E_{52}^{3/2}t_{\rm days}^{-5/2}d_{L28}^{-2}$	$3.44p-1.41$ [a]	0.7 [a]
				$8.08(p-1.22)10^{16}(1+z)^{1/2}\bar{\epsilon}_e^2\epsilon_B^{1/2}E_{52}^{1/2}t_{\rm days}^{-3/2}$	$3.04(p-1.79)10^{15}(1+z)^3\bar{\epsilon}_e^5\epsilon_B A_*^{-1}E_{52}^2 t_{\rm days}^{-2}d_{L28}^{-2}$	$3.63p-1.60$ [a]	1.8 [a]

TABLE 2—*Continued*

b	β_1	β_2	ν_b	$\nu_b(p)$ (Hz)	$F_{\nu_b,\text{ext}}(p)$ (mJy)	$s(p)$	MRD (%)
5.....	$\dfrac{5}{2}$	$\dfrac{1-p}{2}$	ν_{sa}	$3.59(4.03-p)10^9 e^{2.34p}\left[\dfrac{\bar{\epsilon}_e^{4(p-1)}\epsilon_B^{p+2} n_0^4 E_{52}^{p+2}}{(1+z)^{6-p} t_{\text{days}}^{3p+2}}\right]^{1/2(p+4)}$	$20.8(p-1.53)e^{2.56p} d_{L28}^{-2}\left[\dfrac{(1+z)^{7p+3}\epsilon_B^{2p+3} E_{52}^{3p+7}}{\bar{\epsilon}_e^{10(1-p)} t_{\text{days}}^{5(p-1)}}\right]^{1/2(p+4)}$	$1.47-0.21p$	5.9
				$1.58(4.10-p)10^{10} e^{2.16p}\left[\dfrac{\bar{\epsilon}_e^{4(p-1)}\epsilon_B^{p+2} A_*^8}{(1+z)^{2-p} E_{52}^{2-p} t_{\text{days}}^{3(p+2)}}\right]^{1/2(p+4)}$	$158(p-1.48)e^{2.24p} d_{L28}^{-2}\left[\dfrac{(1+z)^{6p+9}\epsilon_B^{2p+3} E_{52}^{4p+1}}{\bar{\epsilon}_e^{10(1-p)} A_*^{2(p-6)} t_{\text{days}}^{4p+1}}\right]^{1/2(p+4)}$	$1.25-0.18p$	7.2
6.....	$\dfrac{5}{2}$	$-\dfrac{p}{2}$	ν_{sa}	$3.23(p-1.76)10^{12}\left[\dfrac{\bar{\epsilon}_e^{4(p-1)}\epsilon_B^{p-1} n_0^2 E_{52}^{p+1}}{(1+z)^{7-p} t_{\text{days}}^{3(p+1)}}\right]^{1/2(p+5)}$	$76.9(p-1.08)e^{2.06p} d_{L28}^{-2}\left[\dfrac{(1+z)^{7p+5}\epsilon_B^{2p-5} E_{52}^{3p+5}}{\bar{\epsilon}_e^{10(1-p)} n_0^p t_{\text{days}}^{5(p-1)}}\right]^{1/2(p+5)}$	$0.94-0.14p$	12.4
				$4.51(p-1.73)10^{12}\left[\dfrac{\bar{\epsilon}_e^{4(p-1)}\epsilon_B^{p-1} A_*^4 E_{52}^{p-1}}{(1+z)^{5-p} t_{\text{days}}^{3p+5}}\right]^{1/2(p+5)}$	$78.6(p-1.12)e^{1.89p} d_{L28}^{-2}\left[\dfrac{(1+z)^{6p+5}\epsilon_B^{2p-5} E_{52}^{4p+5}}{\bar{\epsilon}_e^{10(1-p)} A_*^{2p} t_{\text{days}}^{4p-5}}\right]^{1/2(p+5)}$	$1.04-0.16p$	11.0
7.....	2	$\dfrac{11}{8}$	ν_{ac}	$1.12\dfrac{(3p-1)^{8/5}}{(3p+2)^{8/5}}10^8(1+z)^{-13/10}\bar{\epsilon}_e^{-8/5}\epsilon_B^{-2/5} n_0^{3/10} E_{52}^{-1/10} t_{\text{days}}^{3/10}$	$5.27\dfrac{(3p-1)^{11/5}}{(3p+2)^{11/5}}10^{-3}(1+z)^{-1/10}\bar{\epsilon}_e^{-11/5}\epsilon_B^{-4/5} n_0^{1/10} E_{52}^{3/10} t_{\text{days}}^{11/10} d_{L28}^{-2}$	$1.99-0.04p$	1.9
				$1.68\dfrac{(3p-1)^{8/5}}{(3p+2)^{8/5}}10^8(1+z)^{-1}\bar{\epsilon}_e^{-8/5}\epsilon_B^{-2/5} A_*^{3/5} E_{52}^{-2/5}$	$3.76\dfrac{(3p-1)^{11/5}}{(3p+2)^{11/5}}10^{-3}\bar{\epsilon}_e^{-11/5}\epsilon_B^{-4/5} A_*^{1/5} E_{52}^{1/5} t_{\text{days}} d_{L28}^{-2}$	$1.97-0.04p$	1.9
8.....	$\dfrac{11}{8}$	$-\dfrac{1}{2}$	ν_{sa}	$1.98\times10^{11}(1+z)^{-1/2} n_0^{1/6} E_{52}^{1/6} t_{\text{days}}^{-1/2}$	$154(1+z)\epsilon_B^{-1/4} n_0^{-1/12} E_{52}^{2/3} d_{L28}^{-2}$	0.907	1.71
				$3.15\times10^{11}(1+z)^{-1/3} A_*^{1/3} t_{\text{days}}^{-2/3}$	$119(1+z)^{11/12}\epsilon_B^{-1/4} A_*^{-1/6} E_{52}^{3/4} t_{\text{days}}^{1/12} d_{L28}^{-2}$	0.893	2.29
9.....	$-\dfrac{1}{2}$	$-\dfrac{p}{2}$	ν_m	$3.94(p-0.74)10^{15}(1+z)^{1/2}\bar{\epsilon}_e^2\epsilon_B^{1/2} E_{52}^{1/2} t_{\text{days}}^{-3/2}$	$0.221(6.27-p)(1+z)^{1/2}\bar{\epsilon}_e^{-1}\epsilon_B^{-1/2} E_{52}^{1/2} t_{\text{days}}^{1/2} d_{L28}^{-2}$	$3.34-0.82p$	4.5
				$3.52(p-0.31)10^{15}(1+z)^{1/2}\bar{\epsilon}_e^2\epsilon_B^{1/2} E_{52}^{1/2} t_{\text{days}}^{-3/2}$	$0.165(7.14-p)(1+z)^{1/2}\bar{\epsilon}_e^{-1}\epsilon_B^{-1/2} E_{52}^{1/2} t_{\text{days}}^{1/2} d_{L28}^{-2}$	$3.68-0.89p$	4.2
10...	$\dfrac{11}{8}$	$\dfrac{1}{3}$	ν_{sa}	$1.32\times10^{10}(1+z)^{-1/2}\epsilon_B^{6/5} n_0^{11/10} E_{52}^{7/10} t_{\text{days}}^{-1/2}$	$3.72(1+z)\epsilon_B^{7/5} n_0^{6/5} E_{52}^{7/5} d_{L28}^{-2}$	1.213	5.22
				$\ldots^{\text{b}}$	$\ldots^{\text{b}}$	$\ldots^{\text{b}}$	$\ldots^{\text{b}}$
11...	$\dfrac{1}{3}$	$-\dfrac{1}{2}$	ν_c	$5.86\times10^{12}(1+z)^{-1/2}\epsilon_B^{-3/2} n_0^{-1} E_{52}^{-1/2} t_{\text{days}}^{-1/2}$	$28.4(1+z)\epsilon_B^{1/2} n_0^{1/2} E_{52} d_{L28}^{-2}$	0.597	0.55
				$\ldots^{\text{b}}$	$\ldots^{\text{b}}$	$\ldots^{\text{b}}$	$\ldots^{\text{b}}$

NOTE.—First column numbers the breaks. The following two columns are the asymptotic spectral slopes below (β_1) and above (β_2) the break. The fourth column gives the name of the break frequency. The following two columns are $\nu_b(p)$ and $F_{\nu_b,\text{ext}}(p)$. The last two columns are the parameter $s(p)$, which determines the shape of each break according to eq. (1) (except for $b=4$, where it applies to eq. [3]), and the maximal relative difference (MRD) between this analytic formula and our exact numerical results. For each break frequency there are two lines; the first is for an ISM surrounding ($k=0$) and the second for a stellar wind environment ($k=2$). The reader is reminded that $\bar{\epsilon}_e = \epsilon_e(p-2)/(p-1)$ depends on p.

[a] For $b=4$, the values of $s(p)$ and the corresponding MRD refer to eq. (3), and not to eq. (1) as for the other breaks.

[b] The breaks $b=10,\ 11$ involve PLS E, where the emission is dominated by the contribution from small radii for $k>23/13$. This new regime is described in a separate work (J. Granot & R. Sari 2002, in preparation).

motivated formula

$$F_\nu = F_{\nu_1, \text{ext}}[1 - \exp(-\tau_1)]\tau_1^{-6/5} , \quad \tau_1 = \left(\frac{\nu}{\nu_1}\right)^{-5/3} \quad (2)$$

provides an even better description of F_ν near the break (with a maximal relative difference [MRD] of 2.63%, compared to 6.78% with eq. [1]). For $k = 2$, however, equation (1) provides a better fit (with an MRD of 1.02%, compared to 25% with eq. [2]), which shows that the previous success of equation (2) was accidental.

Both equations (1) and (2) give a poor fit for $b = 4$. This is because the spectral slope across this break does not change monotonically. We therefore provide an alternative formula for this break:

$$F_\nu = F_{\nu_4, \text{ext}} \left[\phi_4^2 \exp(-s\phi_4^{2/3}) + \phi_4^{5/2}\right] , \quad \phi_4 = \frac{\nu}{\nu_4} , \quad (3)$$

where the values of s for $b = 4$ that appear in Table 2 are for this equation rather than for equation (1), as for the other breaks.

4. PRESCRIPTION FOR THE BROADBAND SPECTRA

The values and the shape of the break frequencies, as given in the previous section, are strictly valid only when the break frequencies are far away from each other. Although, in principle, our formalism is adequate to describe the general spectrum, for arbitrary values of the break frequencies, such a description would require a new calculation for any ratio of the break frequencies and is therefore not practical. Instead, we choose to give a heuristic prescription that uses the shapes from the previous section to construct a broadband spectrum, which includes all the breaks for an arbitrary ratio of the break frequencies. Once again, we stress that this is not a rigorous derivation of such a spectrum but simply an analytic equation that gives a smooth spectrum when the break frequencies are close to each other and approaches the rigorous shape of each break in the asymptotic situation in which the break frequencies are far apart. Such an equation is useful for fitting afterglow data.

One can readily construct such a formula for any one of the five different possible spectra shown in Figure 1. Let us label these spectra 1–5, from top to bottom, and denote the corresponding flux densities by $F_\nu^{(i)}$, where $i = 1, \ldots, 5$. We also label the flux density near the 11 spectral breaks by F_b, where $b = 1, \ldots, 11$. The fluxes, F_b, are given by equation (1) (for break $b = 4$, eq. [3] gives a more accurate description). Now, let us define a quantity $\tilde{F}_b$ by

$$\tilde{F}_b = \left[1 + \left(\frac{\nu}{\nu_b}\right)^{s(\beta_1 - \beta_2)}\right]^{-1/s} . \quad (4)$$

The formulas for the rounded shape of the spectrum for the five spectra that are shown in Figure 1, from top to bottom, are given by

$$F_\nu^{(1)} = F_1 \tilde{F}_2 \tilde{F}_3 , \quad (5)$$

$$F_\nu^{(2)} = F_4 \tilde{F}_5 \tilde{F}_3 , \quad (6)$$

$$F_\nu^{(3)} = F_4 \tilde{F}_6 , \quad (7)$$

$$F_\nu^{(4)} = F_7 \tilde{F}_8 \tilde{F}_9 , \quad (8)$$

$$F_\nu^{(5)} = F_7 \tilde{F}_{10} \tilde{F}_{11} \tilde{F}_9 . \quad (9)$$

The first term, F_b, provides the normalization and the shape of the spectrum near the lowest break frequency, while each consecutive term, $\tilde{F}_b$, represents the next break frequency from low to high frequencies and provides the shape of the spectrum near that break frequency and the appropriate change in the spectral slope across the break. The number of free parameters in each spectrum generally equals the number of break frequencies plus 2, since other than the values of the break frequencies, one has to specify the value of p and of the flux normalization. The bottom panel of Figure 1 is an exception, and $F_\nu^{(5)}$ has only five free parameters, since there is a closure relation between the four break frequencies (Granot et al. 2000):

$$\frac{\nu_{10}}{\nu_7}\left(\frac{\nu_{11}}{\nu_9}\right)^{4/5} = h(p) \sim 1 \quad (k = 0) . \quad (10)$$

Our prescription for constructing the broadband spectrum uses $F_{\nu_b, \text{ext}}$ from only one of the break frequencies in each spectrum and thus avoids the problem of the slight inconsistencies within Table 2 (which arise because of the independent fits for the p dependence; e.g., § 3).

5. DISCUSSION

We have used the BM solution to obtain more accurate expressions for the flux density. Under the assumptions that the initial electron distribution is a strict power law with a low-energy cutoff, and that the magnetic field is amplified immediately behind the shock, we derived exact expressions for the values of the break frequencies, as well as the shape of the spectrum around each break. We have given a complete general description of the broadband spectrum. Since our analysis is general, it also includes exotic spectra that may be relevant only in very early phases or for extreme parameters. Our main results are summarized in Figure 1 and Tables 1 and 2.

In general, the spectrum of GRB afterglows evolves from fast to slow cooling.[4] For example, for an ISM with standard parameters (e.g., $n_0 \cong 1$, $E_{52} \cong 1$, $\epsilon_B \cong 0.01$), the initial spectrum is 5, then ν_m crosses ν_c and the spectrum turns into spectrum 1, and finally, when ν_m crosses ν_{sa}, the spectrum turns into spectrum 2. The transition times between the various spectra of Figure 1 can be worked out by equating the various frequencies as given in Table 3. It follows that there are two types of evolution depending on the parameters, as given in the chart below:

$$\text{ISM} = \begin{cases} 5 \to 1 \to 2 & n_0 E_{52}^{4/7} \epsilon_B^{9/7} < 18 , \\ 4 \to 3 \to 2 & n_0 E_{52}^{4/7} \epsilon_B^{9/7} > 18 ; \end{cases}$$

$$\text{wind} = \begin{cases} 4 \to 5 \to 1 \to 2 & A_* \bar{\epsilon}_e^{-1} E_{52}^{-3/7} \epsilon_B^{2/7} > 100 , \\ 4 \to 3 \to 2 & A_* \bar{\epsilon}_e^{-1} E_{52}^{-3/7} \epsilon_B^{2/7} < 100 . \end{cases}$$

The weakest link in our formalism is the assumption of a sharp lower cutoff in the electron distribution. This would affect breaks $b = 1, 2, 4, 7, 9$ (although for $b = 1$, the shape of the break will not be effected, while ν_1 and $F_{\nu_1, \text{ext}}$ may change). Nevertheless, our calculation provides the first self-consistent description of all these breaks. The values

---

[4] This holds for $k < 4$, which includes the cases relevant for the afterglow, $k = 0, 2$.

TABLE 3
Transition Times between the Different Spectra

$i \to j$	Possible Definitions	k	Transition Time ($t_{i \to j}$) (days)
$5 \to 1$ ...	$\nu_2 = \nu_3,\ \nu_9 = \nu_{11},\ \nu_7 = \nu_{10}$	0	$(7.3 \times 10^2 - 1.7 \times 10^3) \times (1+z) \bar{\epsilon}_e^2 \epsilon_B^2 n_0 E_{52}$
		2	$(2.0 \times 10^2 - 7.0 \times 10^2) \times (1+z) \bar{\epsilon}_e \epsilon_B A_*$
$1 \to 2$ ...	$\nu_1 = \nu_2,\ \nu_4 = \nu_5$	0	$(6.1 \times 10^4 - 1.2 \times 10^6) \times (1+z) \bar{\epsilon}_e^2 \epsilon_B^{1/5} n_0^{-2/5} E_{52}^{1/5}$
		2	$(1.2 \times 10^7 - 3.9 \times 10^9) \times (1+z) \bar{\epsilon}_e^{10/3} \epsilon_B^{1/3} A_*^{-4/3} E_{52}$
$4 \to 5$ ...	$\nu_{10} = \nu_{11}$[a]	2	$9.3(1+z) \epsilon_B^{9/7} A_*^2 E_{52}^{-3/7}$
$4 \to 3$ ...	$\nu_4 = \nu_6,\ \nu_7 = \nu_8 = \nu_9$	0	$(2.2 \times 10^4 - 6.3 \times 10^5) \times (1+z) \bar{\epsilon}_e^2 \epsilon_B^{1/2} n_0^{-1/6} E_{52}^{1/3}$
		2	$(1.5 \times 10^5 - 1.1 \times 10^7) \times (1+z) \bar{\epsilon}_e^{12/5} \epsilon_B^{3/5} A_*^{-2/5} E_{52}^{3/5}$
$3 \to 2$ ...	$\nu_3 = \nu_5$	0	$(5.1 \times 10^8 - 1.2 \times 10^9) \times (1+z) \bar{\epsilon}_e^2 \epsilon_B^{(2p+7)/(p-1)} n_2^{(p+6)/(p-1)} E_{52}^{(p+3)/(p-1)}$
		2	$(8.0 - 24) \times (1+z) \bar{\epsilon}_e^{2(p-1)/(2p+5)} \epsilon_B^{(2p+7)/(2p+5)} A_*^{2(p+6)/(2p+5)} E_{52}^{-3/(2p+5)}$

Note.—First column indicates the transition at hand, from spectrum i to spectrum j. The second column lists possible conditions that may be used to define the transition time. The third column is k, which is either 0 or 2, for an ISM or stellar wind environment, respectively. The last column is the transition time, $t_{i \to j}$. There are several different ways to define most of most transition times (see second column), resulting in numerical coefficients that differ by a factor of order unity. The p dependence also varies the numerical coefficients by a factor of order unity. We specify the range of the numerical coefficients for $2.2 < p < 3$ and for the different definitions of each transition (in parentheses).

[a] Expressions for ν_{10} and ν_{11} for $k = 2$ that we used in order to calculate $t_{4 \to 5}$ are taken from J. Granot & R. Sari 2002, in preparation.

and shapes of the rest of the breaks depend only on the assumption of a power-law distribution well above the low-energy cutoff and on the electron cooling. Our description of these breaks ($b = 3, 5, 6, 8, 10, 11$) is therefore more robust. These breaks may still be somewhat affected by the assumption of the magnetic field evolution. In previous papers (GPS99a; GPS99b), however, we have shown that this dependence is relatively weak ($F_{\nu_2, \mathrm{ext}}$ and ν_2 change by up to $\sim 50\%$, while $F_{\nu_1, \mathrm{ext}}$ and ν_1 change only by up to a few percent, where in both cases the shape of the break does not change considerably).

We give a complete description of all possible PLSs and provide exact expressions for the flux density away from the break frequencies. These expression are useful when partial information for the afterglow exists. In general, a spectral slope and a flux at some frequency are sufficient to give some constraint on the afterglow parameters (in PLSs G and H, p would also be needed). For example, if only X-ray data exists, PLS H can be used to extract some information on the underlying parameters, and if only radio data exists, PLS B can be used even if the self-absorption frequency is not observed (i.e., it is above the observed radio frequency).

Expressions for some of the break frequencies and corresponding flux densities already exist in the literature (Waxman 1997; Sari et al. 1998; Wijers & Galama 1999; GPS99a; GPS99b; Granot et al. 2000; Chevalier & Li 2000; Panaitescu & Kumar 2000). Most of these works address the spectrum shown in the upper panel of Figure 1 (spectrum 1). Some works consider emission from one representative point (Waxman 1997; Sari et al. 1998; Wijers & Galama 1999; Granot et al. 2000), while others (Chevalier & Li 2000; Panaitescu & Kumar 2000) use such an assumption to obtain analytic expressions for the break frequencies while using integration over equal arrival time surfaces for detailed calculations of the light curve (GPS99a and GPS99b consider the emission from the entire volume behind the shock for an equal photon arrival time, the same as in this paper).

The values we obtain for the break frequencies and corresponding flux densities are in some cases significantly different than previous estimates (by up to a factor of ~ 70) and are typically different by a factor of a few. For $k = 0$ and $p = 2.5$, our value for ν_2 ($F_{\nu_2, \mathrm{ext}}$), which is better known as ν_m (F_{ν_m}), is a factor of 1.3 (4.2) larger (smaller) than Sari et al. (1998), a factor of 1.5 (3.0) smaller (larger) than Wijers & Galama (1999), a factor of 2.3 (for ν_2) larger than Panaitescu & Kumar (2000), and a factor of 15 (8) smaller (larger) than Waxman (1997). For $p = 2.2$, our value for ν_2 is a factor of 70 smaller than Waxman (1997).[5] Our values for ν_2 and $F_{\nu_2, \mathrm{ext}}$ are only slightly different (by -5.1% and $+1.6\%$, respectively) than GPS99a, the result of a small approximation they made for the local emissivity. Our value for ν_3 (ν_c) is a factor of 2.6 larger than Sari et al. (1998), a factor of 6.4 larger than Wijers & Galama (1999), and a factor of 6.1 larger than Panaitescu & Kumar (2000). Our value for ν_1 (ν_{sa}) is a factor of 1.9 larger than Waxman (1997), a factor of 3.7 smaller than Wijers & Galama (1999), a factor of 2.1 smaller than GPS99b,[6] and almost identical to Panaitescu & Kumar (2000). For $k = 2$ (and $p = 2.5$), our values of ν_1, ν_2, and ν_3 are smaller by factors of 2.5, 1.4, and 1.4, respectively, than Chevalier & Li (2000), while our value for $F_{\nu_2, \mathrm{ext}}$ is larger by a factor of 3.2. Compared to Panaitescu & Kumar (2000), our values for ν_1, ν_2, and ν_3 are larger by only 18%, 21%, and 16%, respectively. Our expressions for

---

[5] This large difference is mainly the result of the fact that Waxman used ϵ_e instead of our $\bar{\epsilon}_e = \epsilon_e (p - 2)/(p - 1)$.

[6] The reason for this difference is as follows: eq. (18) of GPS99b, which is essentially eq. (6.52) of Rybicki & Lightman (1979), misses the term associated with the discontinuity at the lower edge of the electron distribution (at $\gamma_{\min}$) when derived from eq. (6.50) of Rybicki & Lightman. This missing term caused an overestimation of the of the absorption coefficient by a factor of $f = 3(p + 2)/4$ and a corresponding overestimation of ν_1 and $F_{\nu_1, \mathrm{ext}}$, by factors of $f^{3/5}$ and $f^{1/5}$, respectively. However, this missing term does not effect the shape of the break, which is given in eqs. (1) or (2) (i.e., eq. [24] of GPS99b).

the break frequencies and corresponding flux densities of spectra 4 and 5 (bottom two panels of Fig. 1) for $k = 0$, 2 are different by up to a factor of 3 from those given in Granot et al. (2000).

When using our results to determine the afterglow parameters (E_{52}, n_0 or A_*, ϵ_e, ϵ_B, and p) through fits to the observational data, the values of these parameters may differ from previous estimates both because of the different shape of the spectrum and because of the different values of the break frequencies and corresponding flux densities. In order to illustrate the quantitative differences our results may induce when determining the afterglow parameters from such fits, we will use the results of Wijers & Galama (1999) for GRB 970508. They used the values of the break frequencies and peak flux of this afterglow 12.1 days after the burst to determine the afterglow parameters. Replacing their theoretical values for the break frequencies and flux density with ours and keeping their observational values, we find that E_{52} decreases by a factor of 30 (from 3.5 to 0.12), ϵ_e increases by a factor of 4.8 (from 0.12 to 0.57) , ϵ_B decreases by a factor of 7.6 (from 0.089 to 0.012), and n_0 increases by a factor of 730 (!) from 0.03 to 22. Using our broadband spectrum in which the PLSs join smoothly at the break frequencies instead of the broken power-law theoretical spectrum used by Wijers & Galama will also change the values of the break frequencies and peak flux that are inferred from the data. The resulting changes to the values of the afterglow parameters are expected to be of the same order as those quoted above. Therefore, in order to determine the after-glow parameters with reasonable accuracy, one needs to perform a fit to all the available observational data using the prescription for the broadband spectrum that is outlined in § 4. Such a fit, however, is beyond the scope of this paper.

Our equations do not include the effects of inverse Compton scattering on the cooling of the electrons. This effect is known to be important when $\epsilon_B \ll \epsilon_e$ (Sari, Narayan, & Piran 1996; Panaitescu & Kumar 2000; Sari & Esin 2001). Following the prescription of Sari & Esin, we can include the effects of inverse Compton by inserting appropriate powers of $(1 + Y)$ into the values of the break frequencies or the PLSs (where Y is the Compton y-parameter). PLSs C, E, F, and H should be multiplied by $(1 + Y)^{-3/8}$, $(1 + Y)^{2/3}$, $(1 + Y)^{-1}$, and $(1 + Y)^{-1}$, respectively.

Preliminary results from this work have already been used successfully in fitting the data of several afterglows (e.g., Galama et al. 2000; Harrison et al. 2001). In the latter case, the first evidence for inverse Compton emission was found. A special effort has been made to present the results of our model in a way that is simple to implement and would provide the most accurate results to date for spherical afterglows or jetted afterglows within their quasi-spherical phase (before any significant lateral spreading).

APPENDIX

The energy density e, number density n, magnetic field B, and random Lorentz factor of the electrons γ_e are measured in the local rest frame of the fluid in addition to all the primed quantities. The remaining quantities are measured in the lab frame, i.e., the rest frame of the ambient medium in which the flow is spherical. We use a spherical coordinate system in this rest frame, where the z-axis points at the observer. The time, t, measured in this rest frame is called the coordinate time and is to be distinguished from the time, t', measured in the local rest frame of the fluid and from the observer (or observed) time, t_{obs}, at which the emitted photons reach the observer. The subscript 0 denotes the value of a quantity just behind the shock.

The initial electron distribution just behind the shock is given by

$$N(\gamma_e) = K_0 \gamma_e^{-p} \quad \text{for} \quad \gamma_e \geq \gamma_{\min, 0} = \frac{\bar{\epsilon}_e e_0}{n_0 m_e c^2} \;, \tag{A1}$$

where m_e is the electron rest mass and $K_0 = (p - 1) n_0 \gamma_{\min, 0}^{p-1}$. Note that the above equation is usually written using $\epsilon_e = \bar{\epsilon}_e (p - 1)/(p - 2)$, which is the fraction of the internal energy given to the electrons. The advantage of using $\bar{\epsilon}_e$ is that it makes most equations somewhat simpler. Furthermore, it will apply also for the case $p < 2$ as long as the minimal Lorentz factor is proportional to the shock Lorentz factor. The magnetic field is assumed to hold a constant fraction, ϵ_B, of the internal energy, everywhere:

$$B^2 = 8\pi \epsilon_B e \;. \tag{A2}$$

The evolution of the Lorentz factor of each electron is described by

$$\frac{d\gamma_e}{dt'} = -\frac{\sigma_T B^2}{6\pi m_e c} \gamma_e^2 + \frac{\gamma_e}{3n} \frac{dn}{dt'} \;. \tag{A3}$$

The first term on the right-hand side of equation (A3) represents the radiative losses, while the second term represents adiabatic cooling. The radiative term includes only synchrotron losses. A simple prescription of how to include the effects of enhanced electron cooling caused by inverse Compton scattering on the observed synchrotron emission is given in § 5.

We use the BM spherical self-similar solution for an impulsive explosion, where the external medium is cold, and its density changes as a power law of the distance from the center, $\rho_{\mathrm{ext}}(r) = A r^{-k}$, $k < 4$ (extensions for $k > 4$ are given in Best & Sari 2000, but were not used in this paper). The derivations are made for a general value of $k < 4$ and are then used for $k = 0$ and $k = 2$, which are of special physical interest. According to this solution, the proper energy density, Lorentz factor, and proper

number density of the shocked fluid are given by

$$e = 2\Gamma^2 \rho_{\text{ext}} c^2 \chi^{-(17-4k)/3(4-k)} , \tag{A4}$$

$$\gamma = 2^{-1/2} \Gamma \chi^{-1/2} , \tag{A5}$$

$$n = 2^{3/2} \Gamma n_{\text{ext}} \chi^{-(10-3k)/2(4-k)} , \tag{A6}$$

where Γ is the Lorentz factor of the shock, and

$$\chi = \left[1 + 2(4 - k)\Gamma^2 \right] \left(1 - \frac{r}{ct} \right) . \tag{A7}$$

The χ coordinate of a fluid element is given by

$$\chi = \left(\frac{R}{R_0} \right)^{4-k} = \left(\frac{t}{t_0} \right)^{4-k} , \tag{A8}$$

where R_0 and t_0 are the shock radius and coordinate time, respectively, when the fluid element crosses the shock. Since $\Gamma^2 \propto t^{k-3}$, we obtain

$$\frac{\gamma}{\gamma_0} = \chi^{-(7-2k)/2(4-k)} , \qquad \frac{n}{n_0} = \chi^{-(13-2k)/2(4-k)} , \qquad \frac{e}{e_0} = \left(\frac{B}{B_0} \right)^2 = \chi^{-2(13-2k)/3(4-k)} . \tag{A9}$$

Using equation (A9) and the relation $dt' = dt/\gamma$, we can write equation (A3) in terms of χ:

$$\frac{d\gamma_e}{d\chi} = -\frac{\sigma_T B_0^2 t_0 \chi^{-(49-8k)/6(4-k)} \gamma_e^2}{6(4-k)\pi m_e c \gamma_0} - \frac{(13-2k)}{6(4-k)} \frac{\gamma_e}{\chi} . \tag{A10}$$

Solving equation (A10), we obtain

$$\gamma_e(\gamma_{e,0}, \chi) = \frac{\gamma_{e,0}}{\chi^{(13-2k)/6(4-k)} + \gamma_{e,0}/\gamma_{\max}(\chi)} , \tag{A11}$$

where $\gamma_{e,0} \equiv \gamma_e(\chi = 1)$ is the initial Lorentz factor of the electron just behind the shock, and $\gamma_{\max}(\chi)$ is the maximal Lorentz factor at $\chi > 1$, which corresponds to an electron with $\gamma_{e,0} \to \infty$, and is given by

$$\gamma_{\max}(\chi) = \frac{2(19-2k)\pi m_e c \gamma_0}{\sigma_T B_0^2 t_0} \frac{\chi^{(25-2k)/6(4-k)}}{\chi^{(19-2k)/3(4-k)} - 1} . \tag{A12}$$

The fraction of electrons with a Lorentz factor within the interval $[\gamma_e, \gamma_e + d\gamma_e]$ is given by $N(\gamma_e)d\gamma_e/n$ and remains constant as all these quantities evolve with increasing χ. The electron distribution is therefore given by

$$N(\gamma_e, \chi) = K_0 \chi^{(2k-13)(p+2)/6(4-k)} \gamma_e^{-p} \left[1 - \frac{\gamma_e}{\gamma_{\max}(\chi)} \right]^{p-2} \tag{A13}$$

for $\gamma_{\min}(\chi) \leq \gamma_e \leq \gamma_{\max}(\chi)$, where $\gamma_{\min}(\chi) = \gamma_e(\gamma_{\min,0}, \chi)$.

We now have explicit expressions for both the hydrodynamical quantities and the electron distribution over all relevant spacetime, and we can calculate the flux density near the various break frequencies. For breaks that are in the optically thin regime ($b = 2, 3, 9, 11$), one may use the equation

$$F_\nu(t_{\text{obs}}) = \frac{2(4-k)R_l^3(1+z)}{d_L^2} \int_0^1 dy \int_1^{y^{k-4}} d\chi \frac{\chi y^{2(5-k)} P'_{\nu'}(y, \chi, t_{\text{obs}})}{[1 + (7-2k)\chi y^{4-k}]^2} , \tag{A14}$$

which is a generalization of equation (13) of GPS99a, where d_L and z are the luminosity distance and cosmological redshift of the source, respectively, $P'_{\nu'}$ is the radiated power per unit volume per unit frequency in the local rest frame of the fluid and should be taken at the coordinate time $t = t_z + r\mu/c$, where $t_z \equiv t_{\text{obs}}/(1+z)$,

$$R_l = \left[\frac{(17-4k)(4-k)Et_z}{4\pi Ac} \right]^{1/(4-k)} ,$$

$$\gamma_l = \left[\frac{(17-4k)E}{4^{5-k}(4-k)^{3-k}\pi Ac^{5-k}t_z^{3-k}} \right]^{1/2(4-k)} , \tag{A15}$$

E is the energy of the blast wave, $y \equiv R/R_l$ (e.g., GPS99a),

$$\mu \equiv \cos(\theta) \cong 1 - \frac{1 - \chi y^{4-k}}{4(4-k)\gamma_l^2 y} , \tag{A16}$$

and[7] $\nu' = \nu\gamma(1 - \beta\mu)(1 + z)$. The spectral emissivity of a single electron (in the fluid rest frame) is given by

$$P'_{\nu',e} = \frac{\sqrt{3}q_e^3 B \sin\alpha}{m_e c^2} F\left(\frac{\nu'}{\nu'_{\rm syn}}\right) , \quad \nu'_{\rm syn} = \frac{3q_e B \gamma_e^2 \sin\alpha}{4\pi m_e c} , \tag{A17}$$

where q_e is the electric charge of the electron, α is the pitch angle between the direction of the electron's velocity and the magnetic field in the local rest frame of the fluid, and F is the standard synchrotron function (e.g., Rybicki & Lightman 1979). In order to obtain an expression for $P'_{\nu'}$ (which appears in eq. [A14]), we average $P'_{\nu',e}$ over α, assuming an isotropic distribution of electrons in the local rest frame:

$$P'_{\nu',e,\rm iso} = \int_0^{\pi/2} d\alpha \sin\alpha P'_{\nu',e}(\sin\alpha) , \tag{A18}$$

and then integrate over the electron distribution:

$$P'_{\nu'} = \int_{\gamma_{\rm min}}^{\gamma_{\rm max}} d\gamma_e N(\gamma_e) P'_{\nu',e,\rm iso}(\gamma_e) . \tag{A19}$$

For the remaining spectral breaks ($b = 1, 4, 5, 6, 7, 8, 10$), where the system is not always optically thin, we follow the formalism of GPS99b. Since the emission is isotropic in the local rest frame of the fluid, the emission coefficient is simply $j'_{\nu'} = P'_{\nu'}/4\pi$, where $P'_{\nu'}$ is given by equation (A19). The absorption coefficient is given by

$$\alpha'_{\nu'} = \frac{1}{8\pi m_e \nu'^2} \int_{\gamma_{\rm min}}^{\gamma_{\rm max}} d\gamma_e \frac{N(\gamma_e)}{\gamma_e^2} \frac{\partial}{\partial\gamma_e}\left[\gamma_e^2 P'_{\nu',e,\rm iso}(\gamma_e)\right] . \tag{A20}$$

Since the flow is spherically symmetric, the afterglow image is circular, with physical radius of

$$R_{\perp,\rm max} = \frac{(5-k)^{(k-5)/2(4-k)}}{\sqrt{2}} \frac{R_l}{\gamma_l} = \left[\frac{2^{2-k}(17-4k)(4-k)^{5-k}Ec^{3-k}t_z^{5-k}}{\pi(5-k)^{5-k}A}\right]^{1/2(4-k)} , \tag{A21}$$

and for a given observer time, $t_{\rm obs}$, the specific intensity (or brightness), I_ν, depends only on the normalized radius from the center of the image:

$$x \equiv \frac{R_\perp}{R_{\perp,\rm max}} = (4-k)^{-1/2}(5-k)^{(5-k)/2(4-k)}\sqrt{y - \chi y^{5-k}} , \tag{A22}$$

where $x = 0$ at the center of the image and $x = 1$ at the outer edge of the image. As discussed in GPS99b, $I_\nu(x)$ may be obtained by solving the radiative transfer equation:

$$\frac{dI_\nu}{ds} = j_\nu - \alpha_\nu I_\nu , \tag{A23}$$

where s is the distance along the trajectory of a photon to the observer, and the flux density is given by

$$F_\nu(t_{\rm obs}) = 2\pi(1 + z)\left[\frac{R_{\perp,\rm max}(t_{\rm obs})}{d_L}\right]^2 \int_0^1 x \, dx \, I_\nu(x, t_{\rm obs}) . \tag{A24}$$

We note that $I_\nu(x)$ provides the surface brightness profile of the afterglow image that is necessary for detailed calculations of microlensing or scintillation. The surface brightness profiles that were calculated according to this formalism have already been used to study the microlensing of GRB afterglows (Granot & Loeb 2001; Gaudi, Granot, & Loeb 2001) and are presented therein.

When a break frequency is sufficiently far from other break frequencies, the spectrum near this break frequency assumes a self-similar form. These self-similar forms of the spectrum near the different break frequencies are presented in § 3.

---

[7] Here, β is the fluid velocity in units of the speed of light, rather than the spectral index.

REFERENCES

Best, P., & Sari, R. 2000, Phys. Fluids, 12, 3029
Blandford, R. D., & McKee, C. F. 1976, Phys. Fluids, 19, 1130 (BM)
Chevalier, R. A., & Li, Z. Y. 2000, ApJ, 536, 195
Cohen, E., Piran, T., & Sari, R. 1998, ApJ, 509, 717
Galama, T. J., et al. 2000, ApJ, 541, L45
Gaudi, B. S., Granot, J., & Loeb, A. 2001, ApJ, 561, 178
Granot, J., & Königl, A. 2001, ApJ, 560, 145
Granot, J., & Loeb, A. 2001, ApJ, 551, L63
Granot, J., Piran, T., & Sari, R. 1999a, ApJ, 513, 679 (GPS99a)
———. 1999b, ApJ, 527, 236 (GPS99b)
———. 2000, ApJ, 534, L163
Gruzinov, A., & Waxman, E. 1999, ApJ, 511, 852
Harrison, F. A., et al. 2001, ApJ, 559, 123
Panaitescu, A., & Kumar, P. 2000, ApJ, 543, 66
Rybicki, G. B., & Lightman, A. P. 1979, Radiative Processes in Astrophysics (New York: Wiley)
Sari, R. 1997, ApJ, 489, L37
Sari, R., & Esin, A. A. 2001, ApJ, 548, 787
Sari, R., Narayan, R., & Piran, T. 1996, ApJ, 473, 204
Sari, R., Piran, T., & Narayan, R. 1998, ApJ, 497, L17
Waxman, E. 1997, ApJ, 489, L33
Wijers, R. A. M. J., & Galama, T. J. 1999, ApJ, 523, 177